

THE EFFECT OF PRIOR COLD WORK ON TENSILE RESIDUAL STRESS DEVELOPMENT IN NUCLEAR WELDMENTS

Douglas J. Hornbach and Paul S. Prevéy
Lambda Research
5521 Fair Lane
Cincinnati, Ohio 45227

ABSTRACT

Austenitic alloy weldments in nuclear reactor systems are susceptible to stress corrosion cracking (SCC) failures. SCC has been observed for decades and continues to be a primary maintenance concern for both pressurized water and boiling water reactors. SCC can occur if the sum of residual stress and applied stress exceeds a critical threshold tensile stress. Residual stresses developed by prior machining and welding can accelerate or retard SCC depending on their sign and magnitude.

The residual stress, cold work and yield strength distributions on the inside diameter of an Alloy 600 tube J-welded into a pressure vessel were determined by a combination of x-ray diffraction (XRD) and mechanical techniques. A new method was used to relate the XRD line broadening to the percent cold work or true plastic strain in the Alloy 600 tube. The accumulated cold work in the layers deformed by prior machining, in combination with the true stress-strain relationship for Alloy 600, was used to determine the increase in yield strength as a result of deformation due to machining and weld shrinkage. The yield strength of the deformed layer was found to be well in excess of the bulk yield for the alloy, and is therefore capable of supporting residual stresses correspondingly higher.

Tension as high as +700 MPa, exceeding the SCC threshold stress, was observed in both the hoop and axial directions on the inside diameter of the Alloy 600 tubing adjacent to the weld heat affected zone (HAZ). The cold worked high tensile zones correlated with the locations of field SCC failures. The tensile residual stresses are shown to result from a combination of the high cold working from initial machining followed by weld shrinkage. The development of surface tension during weld shrinkage has been modeled using finite element methods, and the benefits of minimizing or removing the cold worked layer prior to welding are demonstrated. Further laboratory studies showing the influence of prior cold working on the formation of residual stresses following bulk plastic deformation are presented.

KEYWORDS: residual stress, stress corrosion cracking, x-ray diffraction (XRD), machining, welding, Alloy 600, finite element analysis, plastic deformation

INTRODUCTION

Stress corrosion cracking (SCC) has been observed for decades on the primary side of austenitic alloy weldments such as 304 stainless steel and Alloy 600. Inspection and maintenance of the weldments continues to be extremely important for proper detection and repair of stress corrosion cracks. Several Alloy 600 J-weld penetrations were observed to have intergranular SCC in both the heater sleeve and pressurized nozzles in nuclear pressure vessels.[1] Residual stress measurements obtained on Alloy 600 sleeves and nozzles prior to welding revealed only stresses less than the +276 MPa threshold stress required to initiate SCC. [2]

To simulate the influences of both machining and welding of the nozzles, several J-weld mockup samples were fabricated. The mockups consisted of Alloy 600 tubular sleeves welded into a carbon steel block. A combination strain gage and XRD method was used to determine both the macroscopic residual stress and cold working on the inside diameter of the nozzle penetration. Layers of material were electropolished from the inside diameter in order to obtain residual stress measurements both at and below the surface within the material deformed by machining. Results obtained in earlier studies, using coarser depth and spatial increments, showed a marked change in both the residual stress and cold working as a function of depth and position.[3,4] Measurements were made at higher depth and spatial resolution in this analysis.

A 2-dimensional finite element model of the J-weld mockup sleeve was used to characterize the effect of prior machining deformation on the final residual stress state after weld shrinkage. The residual stress and yield strength gradients, measured by XRD, were imposed on the inside diameter of the sleeve model to introduce cold working and increased yield strength of the near surface material. Radial displacements were applied to specific areas on the outside diameter of the tube to simulate weld shrinkage.

Controlled laboratory tests were conducted to provide further demonstration of the dramatic influence of prior machining deformation on the formation of residual stress after bulk plastic deformation. Test samples were manufactured from Alloy 718. Due to time constraints Alloy 600 was not used for this test. Alloy 718 was readily available for this demonstration. The group of test samples

was processed to create a surface layer with varying amounts of deformation between each sample. The samples were further deformed in 3-point bending to provide varying amounts of plastic strain along the length of the beam. Residual stress, cold work and yield strength were characterized by XRD both as a function of distance and depth.

SPECIMEN FABRICATION

J-Weld Mockup

Two J-weld heater sleeve mockups were fabricated by ABB-Combustion Engineering in order to simulate the actual fabrication procedures followed in the pressure vessel penetrations that have experienced in-service SCC. An Alloy 600 heater sleeve was taken from decontaminated material, removed from the reactor system, and used for the mockups assuring the same residual stress and deformation as was found in the pressure vessel. The heater sleeve had been cold drawn, and portions of the tube had been reamed during the original pressure vessel assembly.

Each mockup consisted of a carbon steel block with a square base of nominally 152 mm and a 50 deg. penetration angle as shown schematically in Fig. 1. The carbon steel was obtained from archival SA-533B reactor vessel steel. Alloy 82 weld metal was overlaid on the surface to a depth of approximately 10 mm. The penetration clearing was drilled down the center of the block and the J-weld preparations were machined into the Alloy 82 weld metal overlay. The Alloy 600 sleeve was placed into the block and welded in place using the same procedures as followed in the original sleeves which experienced SCC.

Alloy 718 3-Point Bending

Alloy 718 was acquired as 38 x 12.7 mm (1.5 x 0.5 in.) bar stock in the mill annealed condition certified to AMS 5662J and AMS 5596G. The material was solution treated at 982C (1800F) and aged at 732C (1350F) for 8 hrs. + 607C (1125F) for 8 hrs. producing a hardness of 43+/-2 HRC. The aged material had a tensile strength of 1364 MPa (198 ksi), and a 0.2% yield strength of 1109 MPa (161 ksi).

Three beam samples were machined from the bar stock by first saw cutting the samples to 305 mm (12 in.) lengths and further machining the original 12.7 mm (0.5 in.) thickness to 11 mm (0.43 in.) The beam samples remained in the original bar stock width of 38 mm (1.5 in.). Approximately 0.25 mm (0.010 in.) of material was electropolished from both the top and bottom surfaces of the samples to produce a surface layer free of residual stress and cold work.

Two of the three beam samples were processed using surface enhancement methods. The first sample was shot peened in a laboratory peening facility using CW14 steel

shot to a 8A intensity and 100% coverage. The second sample was low plasticity burnished (LPB). The LPB process produces a deep layer of high compression, comparable to laser shock processing (LSP), but with improved surface finish, lower cost, and minimal cold work.[5-9] LPB was performed using a raster pattern with a 19 mm (0.75 in.) ball. The third beam was left in the as-electropolished condition. The three surface conditions (shot peen, LPB and electropolished), produce high, low and zero plastic deformation, respectively, providing a range of surface cold working for comparison of their respective influence on the post-bending residual stresses.

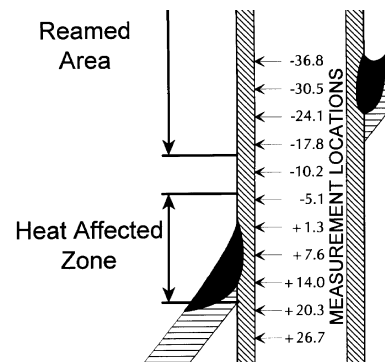
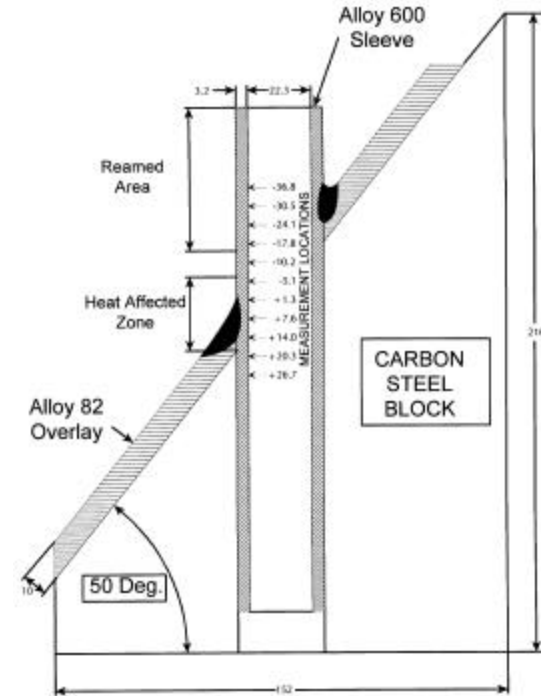


Figure 1 – Alloy 600 50 deg. Heater sleeve penetration J-weld mockup specimen geometry with entire mockup and close-up of measurement locations shown.

EXPERIMENTAL TECHNIQUE

J-Weld Mockup

In order to obtain XRD residual stress measurements on the inside diameter of the Alloy 600 sleeve, the mockup was sectioned. The weld mockup was sectioned axially along a plane perpendicular to the plane of Fig. 1. The “low” and “high” sides of the mockup were then available for residual stress measurement.

The residual stress relaxation that occurred due to sectioning was monitored using strain gage rosettes placed on the inside diameter of the sleeve. A series of six strain gage rosettes were placed on the “low” side of the mockup spanning a total distance of nominally 25 mm. Abrasion of the surface prior to applying the strain gages was not performed to avoid altering the surface and near surface residual stresses. Stress relaxation was interpolated between each strain gage rosette location to provide a continuous distribution of residual stress relaxation at each XRD measurement location.

XRD measurements were made at the locations shown in Fig. 1. The measurements were made on the inside diameter of the Alloy 600 sleeve as a function of axial position. The measurement locations were referenced from the intersection of the plane defining the top surface of the Alloy 82 overlay and the inside diameter surface of Alloy 600 sleeve on the low side.

XRD residual stress measurements were made employing a $\sin^2\psi$ technique and the diffraction of manganese or copper $K\alpha_1$ radiation from the (311) or (420) planes, respectively, of the Alloy 600. It was first verified that the lattice spacing was a linear function of $\sin^2\psi$ as required for the plane stress linear elastic residual stress model. [10-13]

Baseline residual stress measurements were made on the inside diameter of a sleeve prior to welding. Measurements were made using a copper $K\alpha_1$ /(420) technique, in the axial and circumferential directions, in both the reamed and drawn portions of the sleeve. Measurements were made as a function of depth by incremental electropolishing to a final depth of nominally 250 μm . The residual stress measurements were corrected for both the penetration of the radiation into the subsurface stress gradient [14] and for stress relaxation caused by layer removal. [15]

Following the sectioning operation the strain gage rosettes were removed with a chemical epoxy stripper that does not affect the residual stress in the material. XRD residual stress measurements were made in both the hoop and axial directions, along the inside diameter surface of the sleeve, at the measurement locations shown in Fig. 1, as a function of depth to a total depth of nominally 250 μm .

The value of the x-ray elastic constants required to calculate the macroscopic residual stress from the strain

normal to the (311) and (420) planes of the Alloy 600 were determined in accordance with ASTM E1426-91.[16] The x-ray elastic constant $E/(1+\nu)$ for the (311) and (420) planes were 176.6 and 159.3 MPa, respectively. Systematic errors were monitored per ASTM specification E915.

The $K\alpha_1$ peak breadth was calculated from the Pearson VII function fit used for peak location during macroscopic stress measurement.[17] An empirical relationship was established between the material cold working and the $K\alpha_1$ line broadening for Alloy 600. [18] The percent cold work is a scalar quantity, taken to be the true plastic strain necessary to produce the diffraction peak width measured, based on the empirical relationship. The empirical dependence of the $K\alpha_1$ diffraction peak for the (311) diffraction peaks on true plastic strain for Alloy 600 are shown in Fig. 2.

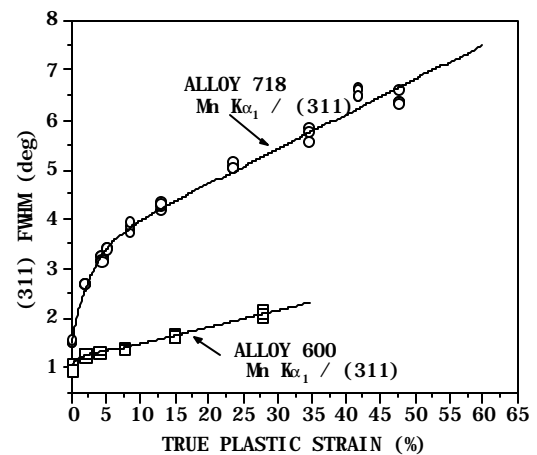


Figure 2 - Empirical relationship between (311) peak width and cold working (true plastic strain) for Alloy 600 and Alloy 718.

The yield strength of Alloy 600 can be estimated at each measurement location from percent cold work and a true stress-strain curve for this alloy. The deformation resulting from the machining operation can exceed 50% true plastic strain and will cause an increase in the yield strength. The true stress-strain curve for the specific Alloy 600 involved in the field SCC failures is shown in Fig. 3. The bulk 0.2% yield strength is nominally 434 MPa. The yield strength doubles at a plastic strain of nominally 25%. The cumulative cold work produced by machining the inside diameter of the sleeve was higher than the 27% limit for this true stress-strain curve and therefore was extrapolated for the purposes of estimating the yield strengths at the higher cold working levels. The ultimate tensile strength (UTS) will also increase as a result of cold working. The published UTS for annealed tubing is 772 MPa which is well below the yield strength at the higher levels of cold working.[19-20]

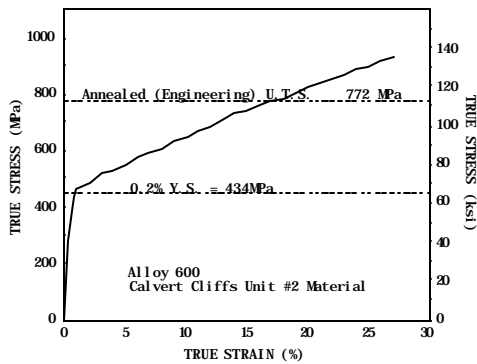


Figure 3 - True stress-strain curve for Alloy 600 heater sleeve material removed from service.

Alloy 718 3-Point Bending

The 3-point bend fixture, shown schematically in Fig. 4, was used to deform the beam samples to known amounts of plastic deformation. The fixture consists of a steel base supporting two adjustable 12.7 mm (0.5 in.) diameter hardened tool steel rollers for the outer supports and a single central roller. The center roller is supported by a 75 x 102 x 102 mm (3 x 4 x 4 in.) cold rolled steel fixture. For this analysis a span of 127 mm (5 in.), between the center and either outer roller, was used. A total deflection of 38.1 mm (1.5 in.) was placed on the center of the beam under displacement control in a servo-hydraulic test machine. Load versus displacement data were recorded for each sample.

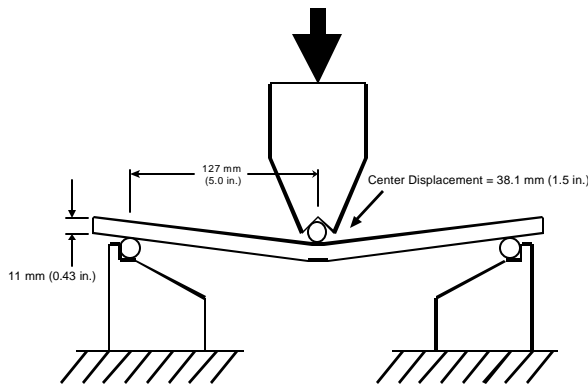


Figure 4 - 3-point bend setup for Alloy 718 beam samples.

XRD residual stress and cold working measurements were obtained in the shot peened and LPB sample, in the longitudinal direction, as a function of depth in an area of the beam that was undeformed by the bending process. These results served as a baseline set of data for comparison to the results in areas deformed by the bending process and for input to a finite element model of the beam. Measurement depths were chosen to best define the entire

compressive residual stress profile and to capture any high stress and cold work gradients that existed. A surface measurement was made to verify the electropolished sample had negligible residual stress and cold working.

XRD surface residual stress measurements were made as a function of position from the center of the bend on all three samples. An automated translation device, capable of collecting a large volume of measurements in a relatively small amount of time with minimal technician interaction, was used for the surface measurements.[21] Measurements were made in the longitudinal direction on the convex side of the sample. The convex side of the sample was deformed in longitudinal tension during bending.

The yield strength of Alloy 718 can be estimated at each measurement location, from the percent cold working and a true stress-strain curve, as discussed earlier. The true stress-strain curve for the Alloy 718 bar stock material used in the 3-point bend experiment is shown in Fig. 5.

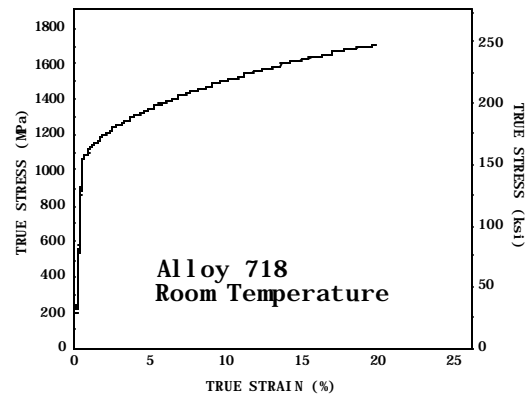


Figure 5 - True stress-strain curve for aged Alloy 718 3-point bend beam material.

FINITE ELEMENT ANALYSIS

J-Weld Sleeve

Finite element methods were used to analytically estimate the influence of the yield strength gradient on the formation of the residual stress distribution caused by weld shrinkage. A 2-dimensional axisymmetric finite element model of the Alloy 600 sleeve was constructed. Residual stress, cold work and yield strength results, obtained by the XRD, were placed in the model to properly account for their influence on the final residual stress distribution caused by weld shrinkage.

It was not the intent of this analysis to directly simulate the precise weld deposition sequence implemented for this mockup. The complex residual stress distribution, measured by XRD, arose from a history of multiple factors such as thermal heat inputs, weld fusion and shrinkage

during weld buildup. The weld deposition sequence and rate of deposition, all that are important factors in the final residual stress formation, were not known.

Dimensions of the sleeve model were the same as that of the mockup. The sleeve had nominal inside diameter dimensions of 22.3 mm (0.88 in.) with a wall thickness of 3.2 mm (0.13 in.) and an overall length of 145 mm (5.71 in.) A cylindrical coordinate system was used with the z-axis coinciding with the axis of the tube.

The sleeve was modeled assuming axisymmetric conditions. Radial displacements were placed on the outside diameter of the sleeve, over an axial span of 60 mm, to simulate the weld shrinkage. Displacement magnitudes were adjusted to produce the nominal levels of bulk cold working from weld shrinkage measured by XRD in the J-weld sleeve.

The sleeve model consisted of over 1500 axisymmetric elements. FEMAP v6.0 commercial software was used to mesh the sleeve model. Higher order elements with mid-side nodes were used in order to capture high strain gradients occurring as a function of position. Relatively small element sizes, on the order of 25 μm , were used on the inside diameter of the tube so the residual stress and yield strength gradients could be properly imposed.

The mechanical material properties of Alloy 600 were obtained from the true stress-strain curve for the alloy shown in Fig. 4. The tabulated data for the true stress vs. strain relationship were placed in the finite element input file. The material deformation was assumed to behave according to the Von-Mises yield criteria.[22-24] Abaqus v6.1 post processing software was used for the analysis.

Alloy 718 3-Point Bending

Prediction of the residual stress state produced by the bending operation was attempted through a finite element model of the beam sample. The purpose of the beam model was to determine how accurately the post-bend residual stresses could be predicted by properly defining the near surface yield strength gradient in the model's material property data of the input file.

A 3-dimensional finite element model of the beam was made. Dimensions of the model matched those of the test samples discussed earlier. Half of the beam was modeled assuming symmetry about the center of bending. The model contained 4920 brick elements with 5709 nodes. FEMAP v6.0 pre-processing software was used to generate the mesh. In order to define the relatively shallow residual stress and yield strength gradients in the surface layers, a fine mesh was used on both the top and bottom sides of the model.

Displacements were prescribed on the nodes along a line corresponding to the line of contact of the center roller of the 3-point bend fixturing. The nodes were displaced a distance of 38.1 mm (1.5 in.), duplicating the displacement

used in the bending of the beam samples. Nodes were constrained along a line corresponding to the line of contact with the outer roller, 127 mm (5 in.) from the center of the bend.

Residual stress and yield strength gradients, measured by XRD, were used to modify the material properties of those elements corresponding to the surface layer deformed by either shot peening or LPB. A bi-linear stress-strain relationship was assumed. The Von Mises yield criteria was assumed.[22-24] Abaqus v6.1 commercial software was used for the analysis.

RESULTS

J-Weld Mockup

The residual stress results obtained on the inside diameter of the drawn and reamed tube sample are shown in Fig. 6. Surface compression exists in both the drawn and reamed portion of the tube. The drawn area of the tube is compressive in both directions to a nominal depth of 125 μm . After reaming the circumferential residual stresses become less compressive and the axial residual stresses become more compressive. The depth of the axial compressive stress is much deeper after the reaming process.

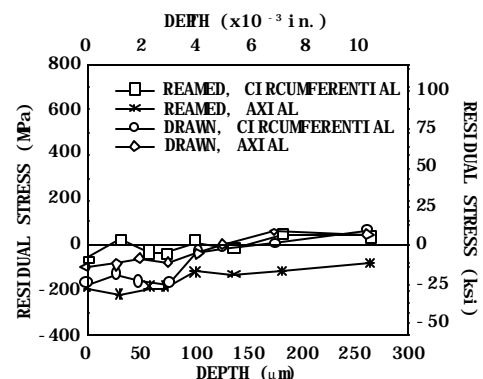


Figure 6 - Baseline subsurface axial and circumferential residual stress for drawn and reamed Alloy 600 sleeve removed from service.

Percent cold work and yield strength subsurface distributions obtained on the baseline Alloy 600 sleeve are shown in Fig. 7. Both the drawing and reaming process produce maximum cold working at the surface, although the surface cold working is nominally twice as high from reaming. The data show that the reaming operation can produce cold working in excess of 50%. The surface of the reamed region has a corresponding increase in yield strength of nominally 600 MPa above the mill annealed yield strength. Both the drawn and reamed areas have a layer of material with an elevated yield strength as a result of prior surface deformation. It will be shown that the near

surface yield strength gradient has a predominant influence on the residual stress field after welding.

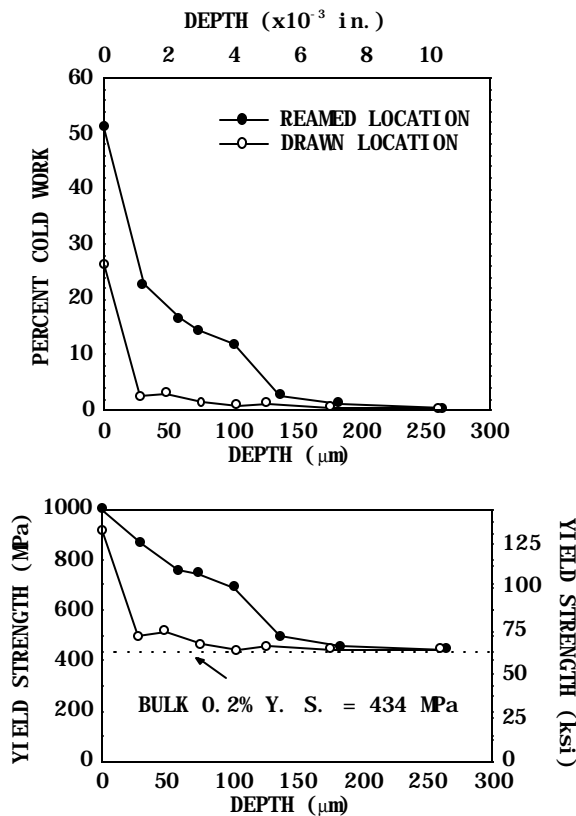


Figure 7 – Subsurface cold work (true plastic strain) and yield strength distributions, demonstrating a marked increase in yield strength in the surface layer, for baseline drawn and reamed Alloy 600 sleeve removed from service.

The cold work and yield strength distributions measured on the inside diameter of the welded sleeve are shown in Figs. 8 and 9, respectively. The results are plotted as a function of axial distance for the various depths tested. The highest cold working is located at the surface in the reamed region of the sleeve. Cold working, on the order of 60%, is found away from the welded area, comparable to those measured on the as-reamed baseline sample. The cold working reaches a maximum at the end of the reamed zone at the surface and to a depth of 51 μm . This maximum can be attributed to the combined cold working from the reaming and weld shrinkage. Cold working from the reaming process is nearly zero at the 254 μm depth. Heat input from the welding process has annealed the material at levels deeper than 25 μm in the HAZ. Cold working as high as 5%, in the deeper levels, nominally 25 mm on either side of the fusion line, is attributed to weld shrinkage.

The yield strength results exceed 1000 MPa at the surface of the reamed zone. The material at the surface and at the 13 μm depth is capable of supporting residual stresses of over 500 MPa as a result of cold working during reaming and weld shrinkage.

The axial residual stress results are shown, as a function of axial position and depth, in Fig. 10. Tensile residual stresses are observed at all of the negative distances from the fusion line. A peak tensile stress exists at the edge of the reamed zone at the surface. This can be attributed to both the high yield strength due to cold working and deformation due to weld shrinkage. The tensile stress in the reamed area increases as a function of depth. The tension at the greater depths is attributed to weld shrinkage. The stresses exceed the SCC threshold at all of the depths, between the -17 and -25 mm locations. Compressive residual stresses are found in the center of the HAZ. However, tensile stresses exist near the edge and outside the HAZ inside the block.

The circumferential residual stress distribution, shown in Fig. 11, is mostly tensile for all the depths and locations tested. The maximum circumferential tension is found at the 13 micron depth near the edge of the reamed area. At the 254 μm depth the Alloy 600 material is in high magnitude uniform tension throughout the weld region. A uniform transition from tension to compression is found near the edge of the HAZ inside the block.

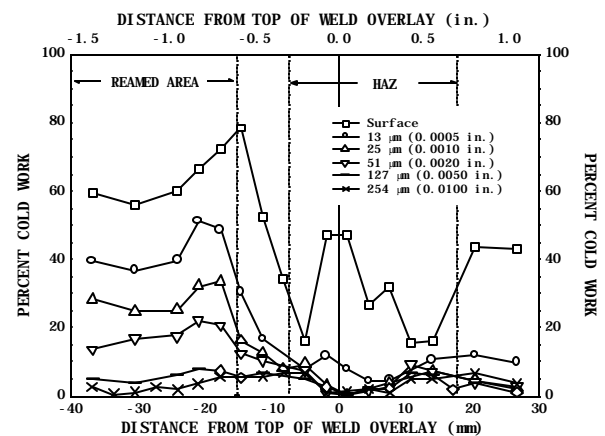


Figure 8 – Variation in cold work (true plastic strain) with axial position on the inside diameter low angle side, of the Alloy 600 J-weld mockup sleeve.

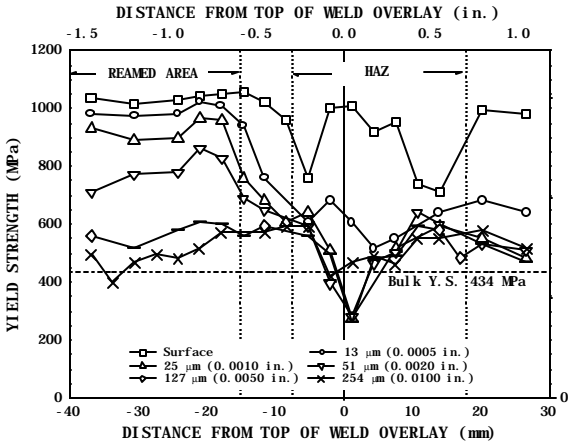


Figure 9 – Variation in yield strength with axial position and depth in HAZ and surrounding regions of the low angle side of the Alloy 600 J-weld mockup sleeve, relative to the bulk yield strength.

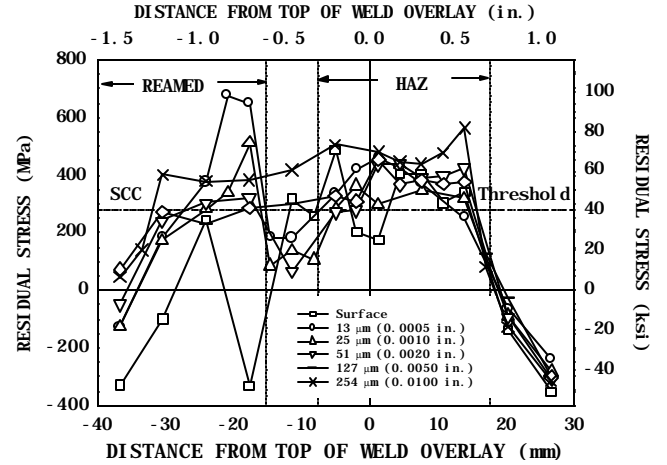


Figure 11 - Variation in circumferential residual stress with axial displacement and depth on the low angle side of the Alloy 600 J-weld mockup sleeve show stresses in excess of the SCC threshold

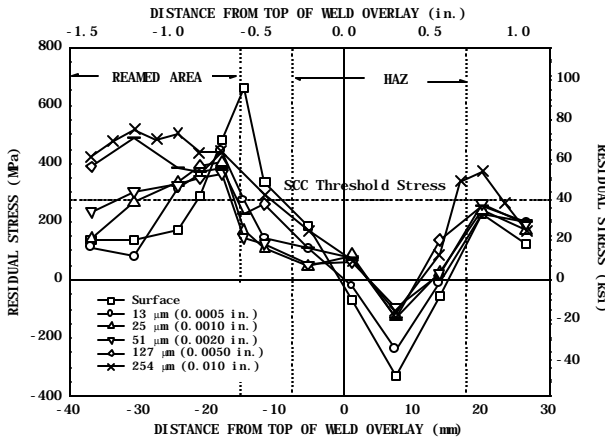


Figure 10 – Variation in axial residual stress with axial position and depth through the HAZ and machined regions on the low-angle side of the Alloy 600 J-weld mockup sleeve showing residual stresses in excess of the SCC threshold.

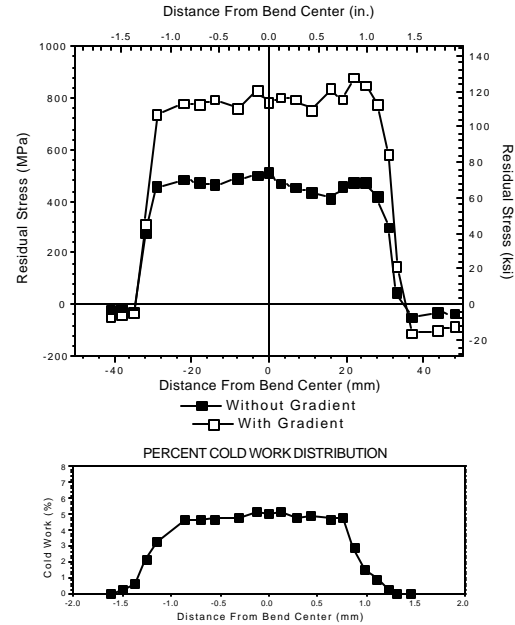


Figure 12 - Finite element residual stress prediction on the inside diameter of the J-weld mockup sleeve model showing a large increase in hoop residual stress when the residual stress and cold working from prior machining are introduced.

Hoop residual stress and plastic strain results, generated with the finite element sleeve model, are shown in Fig. 12. Cold working on the order of 5%, similar to that measured on the J-weld sleeve, was produced over an axial distance of nominally 60 mm of the sleeve model. Hoop residual stresses were markedly higher in the model that included for the yield strength gradient produced by reaming. Residual stresses increased nominally 400 MPa in the deformed region. The results verify that prior cold working has a dramatic influence on weld related residual stresses and that the resulting yield strength distributions must be taken into account to accurately model residual stress formation. Furthermore, the finite element model results imply that minimization of surface cold working will result in minimal tensile stress.

Alloy 718 3-Point Bending

Baseline residual stress and cold work distributions for the Alloy 718 3-point bend beam samples are shown in Fig. 13. As expected the shot peening process produced over 35% cold working at the surface with a compressive layer nominally 200 μm deep. Shot peening produced 15 times more cold working than the LPB process. The depth of

compression was seven times deeper for the LPB process. A surface XRD measurement on the electropolished beam verified there was no cold working and the residual stress was negligible. The range of induced cold working within the group of samples was chosen to provide a comprehensive investigation of the effect of cold work on residual stress following subsequent deformation.

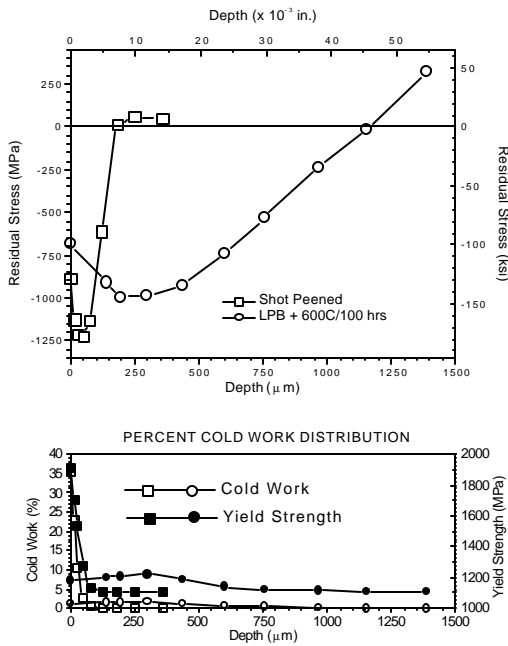


Figure 13 - Subsurface residual stress, cold work and yield strength distributions in baseline region of shot peened and LPB 3-point bend Alloy 718 beam samples.

Surface residual stress distributions obtained on the convex side of the beam samples, measured with the automated translation device, are shown in Fig. 14. Tensile stresses as high as +600 MPa exist at the higher levels of plastic strain from bending near the center of the beam. Tensile residual stresses in the shot peened sample decrease as the bending deformation decreases. Compressive residual stresses would normally be expected on the side of a homogeneous beam deformed in tension with no prior cold working, which is observed for the electropolished and LPB samples. However, this is not the case for the shot peened sample, which has relatively high cold working and correspondingly high yield strength at, and near, the surface. Plastic deformation during machining or surface enhancement of components that will experience further deformation from weld shrinkage should be minimized.

The bar chart in Fig. 15 summarized the dramatic differences in surface residual stress before and after tensile deformation. Residual stresses, at a distance of 14 mm (0.55 in.) from the center of the bend, where deformation from bending was nominally 2.0%, are compared. An increase in compression, from near zero before bending to

nominally -500 MPa after bending is observed for the electropolished sample. The LPB sample experiences a moderate decrease in compression after bending. A marked difference is observed in the residual stress before and after bending of the shot peening sample. This difference can be attributed entirely to the yield strength increase due to the high surface deformation during shot peening.

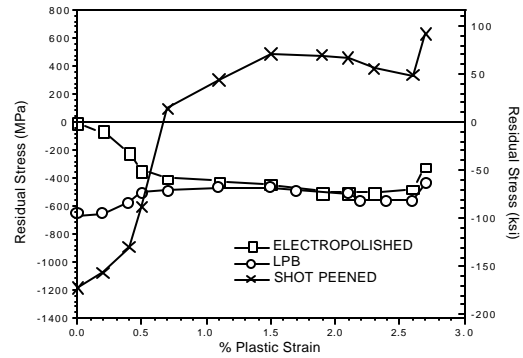


Figure 14 - XRD surface residual stress variation on plastic strain imposed by 3-point bending on convex side of Alloy 718 beam samples.

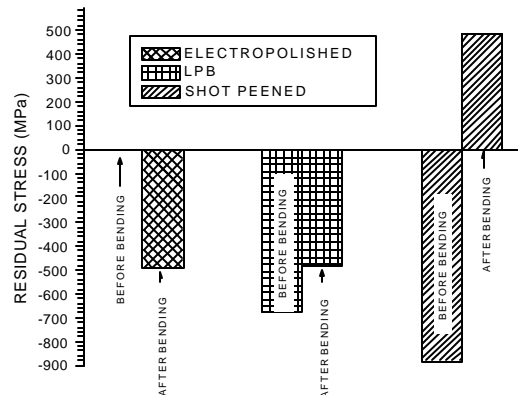


Figure 15 - Comparison of XRD surface residual stress before and after tensile plastic deformation of Alloy 718 beam samples showing an inversion from compression to tension on highly cold worked shot peened sample

Comparison of the residual stresses, both measured by XRD and predicted with FEA, for the electropolished, LPB and shot peened Alloy 718 beams after bending, are shown in Figure 16. Residual stresses are shown as a function of bending plastic strain. The results indicate good agreement between the measured and the finite element predicted stresses when both the yield strength and residual stress gradients are used in the model. If the yield strength gradient is omitted from the model and only the residual stress gradient is considered the predicted results are in considerable error. Small differences between the x-ray and FEA results are probably a result of either slight

differences between the actual material properties of the beams and those prescribed in the material model and the assumption that material plasticity will behave in accordance with the Von Mises yield criteria. The Von Mises yield criteria assumes the material is perfectly isotropic and that the yield strength is the same in tension and compression. [22-24] It has been shown that Alloy 718 is not isotropic and has yield strengths in tension and compression that differ by 30%. [25]

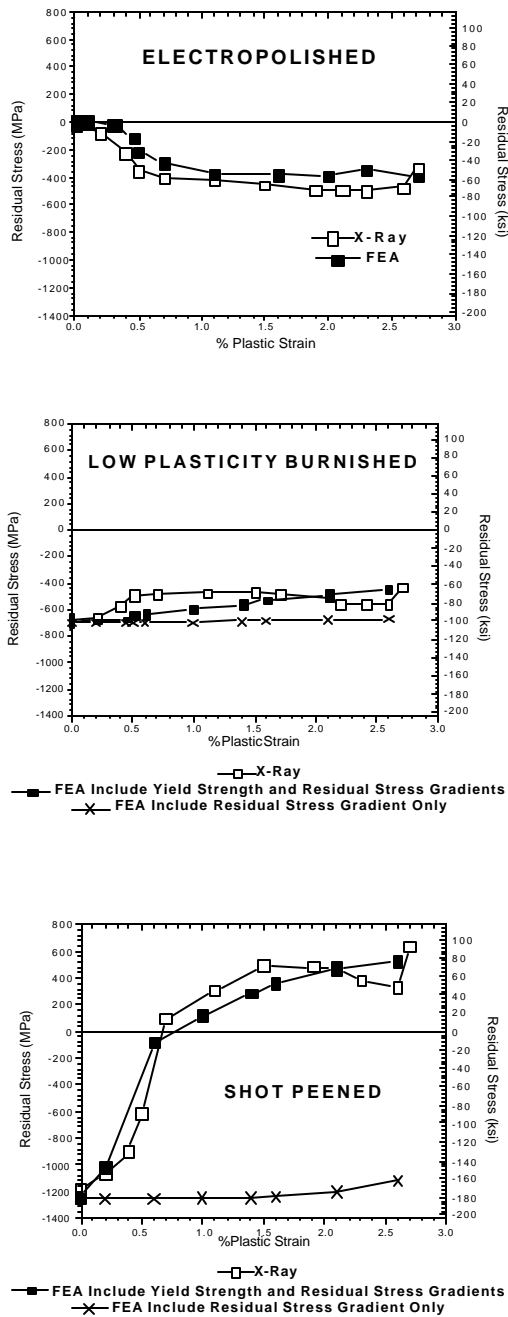


Figure 16 - Comparison of X-ray and FE surface results on electropolished, LPB and shot peened Alloy 718 3-point bend samples.

The comparison of the measured and modeled residual stress distribution after deformation indicates that the previous machining and cold working of the surface layer, or any non-homogeneous material properties must be considered. Finite element predictions would be in considerable error, especially in the case of the shot peened sample, if the residual stress and yield strength gradients were not included in the analysis. Surface compression would be predicted, where in fact they tension exists near the center of the bend of the shot peened sample, if the surface residual and yield strength gradients were not considered.

CONCLUSIONS

The XRD and finite element study of the residual stress, cold work and yield strength due to bulk plastic deformation from weld shrinkage and controlled 3-point bending show a strong influence of the prior deformation from machining and surface enhancement processes on the residual stress state developed. A number of conclusions are supported from the study:

- ◆ Machining and surface enhancement methods can produce cold work in excess of 50%, leading to a dramatic yield strength increase in the deformed surface layers.
- ◆ The inside diameter surface of the Alloy 600 sleeve has an increased yield strength due to machining, and is capable of supporting tensile stresses from weld shrinkage well above that of the bulk material yield strength, resulting in an increased susceptibility to SCC.
- ◆ The influence of the increased yield strength in the deformed surface layer on the final residual stress state can be accurately calculated using finite element methods, provided the yield strength gradient is included.
- ◆ For accurate finite element predictions the residual stress, cold working and yield strength gradients from prior machining must be taken into account.
- ◆ Machining and surface enhancement techniques that produce minimal deformation should be used in areas that will experience further bulk plastic deformation such as in and around weld fusion zones.

REFERENCES

1. Hall, J.F. and Scott, D.B., (1989), "Destructive Examination of Pressurizer Heater Sleeves from Calvert Cliffs Unit 2, *Report CE-NPSD-577*.
2. Gorman, J.A., (1986), "Status and Suggested Course of Action for Nondenting-Related Primary-Side IGSCD of Westinghouse-Type Steam Generators," *EPRI, Report MP-4594-LD*.
3. Hall, J.F., Molkenthin, J.P., and Prevý, P.S., (1993), "XRD Residual Stress Measurements on Alloy 600 Pressurizer Heater Sleeve Mockups," *Proceedings of*

- the Sixth International Symposium on Environmental Degradation of Materials in Nuclear Power Systems-Water Reactors*, (San Diego, CA: TMS, ANS, NACE), pp 855-861.
4. Hall, J.F., Molkenhuth, J.P., Prevéy, P.S. and Pathania, R.S., (1994), "Measurement of Residual Stresses in Alloy 600 Pressurizer Penetrations," *Conference on the Contribution of Materials Investigation to the Resolution of Problems Encountered in Pressurized Water Reactors*, (Paris: Societe Francaise d'Energie Nucleaire, Sept. 12-16).
 5. US Patent 5,826,453 (Oct. 1998).
 6. Prevey, P.S., (2000), "The Effect of Cold Work on the Thermal Stability of Residual Compression in Surface Enhanced IN718," (St. Louis, Missouri, 20th ASM Materials Solutions Conference & Exposition, Oct. 10-12).
 7. Prevey, P.S., Telesman, J., Gabb T., and Kantzos, P., (2000), "FOD Resistance and Fatigue Crack Arrest in Low Plasticity Burnished IN718," (Chandler, AZ, 5th National Turbine Engine High Cycle Fatigue Conference, March 7-9).
 8. Prevey, P.S., and Cammet, J., (2000) "Low Cost Corrosion Damage Mitigation and Improved Fatigue Performance of Low Plasticity Burnished 7075-T6," (Solomons, MD, 4th International Aircraft Corrosion Workshop, Oct.).
 9. (200) "Diffraction Notes, Effect of Low Plasticity Burnishing (LPB) on the HCF Life of IN718," (No. 26 Spring).
 10. Hilley, M.E. ed.,(1971), Residual Stress Measurement by X-Ray Diffraction, SAE J784a, (Warrendale, PA: Society of Auto. Eng.).
 11. Noyan, I.C. and Cohen, J.B., (1987) Residual Stress Measurement by Diffraction and Interpretation, (New York, NY: Springer-Verlag).
 12. Cullity, B.D., (1978) Elements of X-ray Diffraction, 2nd ed., (Reading, MA: Addison-Wesley), pp. 447-476.
 13. Prevéy, P.S., (1986), "X-Ray Diffraction Residual Stress Techniques," *Metals Handbook*, **10**, (Metals Park, OH: ASM), pp 380-392.
 14. Koistinen, D.P. and Marburger, R.E., (1964), Transactions of the ASM, **67**.
 15. Moore, M.G. and Evans, W.P., (1958) "Mathematical Correction for Stress in Removed Layers in X-Ray Diffraction Residual Stress Analysis," SAE Transactions, **66**, pp. 340-345
 16. Prevéy, P.S., (1977), "A Method of Determining Elastic Properties of Alloys in Selected Crystallographic Directions for X-Ray Diffraction Residual Stress Measurement," Adv. In X-Ray Analysis, **20**, (New York, NY: Plenum Press, 1977), pp 345-354.
 17. Prevéy, P.S., (1986) "The Use of Pearson VII Functions in X-Ray Diffraction Residual Stress Measurement," Adv. in X-Ray Analysis, **29**, (New York, NY: Plenum Press), pp 103-112.
 18. Prevey, P.S., (1987), "The Measurement of Residual Stress and Cold Work Distributions in Nickel Base Alloys," Residual Stress in Design, Process and Material Selection, (Metals Park, OH: ASM).
 19. Alloy Digest, (1972), Inconel Alloy 600 Spec. Sheet Ni-176, (Upper Montclair, NJ: Eng. Alloys Dig., July).
 20. Woldman's Engineering Alloys, (1979), 6th Edition, R.C. Gibbons, Ed., American Society for Metals, p. 747.
 21. Diffraction Notes, Residual Stress Contour Mapping, (No. 19, Summer 1997)
 22. Hill, R., (1950), The Mathematical Theory of Plasticity, (Oxford at the Clarendon Press), pp. 19-23
 23. Chen, W.F. and Zhang, H., (1991) Structural Plasticity, pp. 129-130.
 24. Cook, R.D. and Young, W.C., (1985), Advanced Mechanics of Materials, pp. 21-26.
 25. Lissenden, C. J., Gil, C.M., and Lerch B.A., (1999) "A Methodology for Determining Rate-Dependent Flow Surfaces for Inconel 718," Journal of Testing and Evaluation, JTEVA, **27**, No. 6, November, pp. 402-411.